JOURNAL OF SOLID STATE CHEMISTRY 71, 1–11 (1987)

High- and Low-Temperature Phases of Lithium Boron Nitride, Li_3BN_2: Preparation, Phase Relation, Crystal Structure, and Ionic Conductivity

HISANORI YAMANE, SHINICHI KIKKAWA,* AND MITSUE KOIZUMI

The Institute of Scientific and Industrial Research, Osaka University, 8-1 Mihogaoka, Ibaraki, Osaka 567, Japan

Received May 27, 1986

Low- (α) and high- (β) temperature phases of Li_3BN_2 were prepared from mixtures of $Li_3N/BN = 1.1$–1.0 in molar ratio at 1070 and 1170 K, respectively. Phase relation between these phases was studied by annealing the products at various temperatures and conducting DTA in a stream of nitrogen. The phase transition temperature is at about 1135 K. The melting point of β-Li_3BN_2 is around 1189 K. α-Li_3BN_2 crystallizes directly from the undercooled liquid at 1160 K. The structure of α-Li_3BN_2, which is analyzed in the present study for the first time, has tetragonal symmetry, $P4_22_12$, $a = b = 4.6435(2)$, $c = 5.2592(5)$ Å, $Z = 2$, $D_{calc} = 1.747$ Mg m^{-3}, $\mu = 0.082$ mm^{-1}. The structure was determined by 208 unique X-ray reflections with $F_o > 3\sigma(F_o)$ and refined up to $R = 0.042$ by a full-matrix least-squares method. The lattice is composed of Li(1), Li(2), and linear $(NBN)^{3-}$ ions [r(B–N) = 1.339(2) Å]. The Li(1) ion is also linearly coordinated by two nitrogen atoms [r(Li(1)–N = 1.945(8) Å]. The Li(2) ion is at the center of a tetrahedron of N atoms [r(Li(2)–N) = 2.125(18) Å, δ(N–Li–N) = 103.6(2) and 112.5(9)°]. Lithium ion conductivity of 3×10^{-5} S m^{-1} was measured at 400 K on a polycrystalline α-Li_3BN_2 specimen with an activation energy of 78 kJ/mole.

Introduction

The binary system of Li_3N–BN was first studied by Goubeau and Anselment (*1*). They claimed the presence of an $(N{=}B{=}N)^{3-}$ ion in the ternary metal–boron nitride using infrared spectroscopy. DeVries and Fleisher (*2*) synthesized a high-pressure phase of Li_3BN_2. They also reported a pressure–temperature formation diagram for these phases. They presumed that the structures of the high- and low-pressure phases could be related to the anti-fluorite structure of Li_3AlN_2 (*3*).

Another polymorph was recently found by a slow cooling of the melt in a flow of nitrogen. Its crystal structure was analyzed by single-crystal X-ray diffractometry in a preceding manuscript (*4*). However, the phase relations between these two ambient-pressure phases have not been clear. The crystal structure has not been previously reported for the above-mentioned phase prepared by Goubeau and Anselment. The old and new polymorphs of Li_3BN_2 are denoted as α- and β-phases respectively in the present manuscript.

In this paper we first report the preparation of the Li_3N–BN binary compounds. Phase relations are then examined between

* To whom correspondence should be addressed.

0022-4596/87 $3.00

TABLE I

REACTION CONDITIONS AND PRODUCTS IN THE Li_3N–BN SYSTEM

No.	Li_3N/BN[a]	Time (min)	T (K)	Products[b]
1	2.0	10	1070	Li_3N, α-Li_3BN_2, (Li_2O)
2	1.5	60	1070	Li_3N, α-Li_3BN_2, (Li_2O)
3	1.1	60	1070	α-Li_3BN_2, (Li_2O)
4	0.7	80	1070	α-Li_3BN_2, Li–BN, (Li_2O)
5	0.3	150	1340	Li–BN, α-Li_3BN_2
6	0.2	60	1220	BN, Li–BN, α-Li_3BN_2
7	1.1–1.0	10	1270	α-Li_3BN_2, (Li_2O)
8	1.1–1.0	10	1170	β-Li_3BN_2, (Li_2O)
9	1.1–1.0	10	1070	α-Li_3BN_2, (Li_2O)
10	1.1–1.0	10	970	α-Li_3BN_2, Li_3N, BN, (Li_3N)

[a] Molar ratio in the starting mixture.
[b] See Table II for X-ray powder data.

α- and β-Li_3BN_2. The crystal structure of α-Li_3BN_2 is also reported by single-crystal X-ray diffractometry. The measured ionic conductivity of α-Li_3BN_2 is compared with that of β-Li_3BN_2.

Experimental

Lithium nitride was prepared by a reaction of nitrogen gas (Osaka Oxygen Ind. Ltd., 99.999%) with lithium (Wako Pure Chemical Ind. Ltd., 99%) in a temperature range of 373–473 K. Pulverized Li_3N was mixed with boron nitride powder (Showa Denko Co., 99.8%) in various molar ratios as shown in Table I. The starting mixtures were compressed to a pellet and enclosed in tantalum foils. These operations were carried out in a helium-filled glove box. The pellets were heated in a stream of nitrogen in the desired reaction conditions as shown in Table I and quenched in the furnace to room temperature. The estimated rate of temperature decrease was about 100 K/min above 800 K. The phases in the products were identified by X-ray powder diffractometry. X-ray powder diffraction data were obtained by means of a goniometer (r = 185 mm) using CuK_α (1.5418 Å) radiation monochromatized with pyrolytic graphite.

Differential thermal analysis was carried out using an alumel–chromel thermocouple in a stream of nitrogen. The heating rate was 20 K/min and α-Al_2O_3 was used as a reference. Samples of 3–5 mg and the reference were encapsuled in tantalum foils.

Single crystals of α-Li_3BN_2 for structural analysis were prepared from the starting mixture, which had a molar ratio Li_3N/BN = 1.0–1.2. The mixture was heated at 1300 K for 20 min and cooled to 1000 K at a rate of about 2 K/min. A single crystal with a size of 0.15 × 0.1 × 0.1 mm was obtained by crushing the massive product. The crystal had an irregularly angular shape with a glassy and white surface. It was sealed with argon gas in a glass capillary because of its instability with respect to moisture.

Oscillation and Weissenberg photographs taken with CuK_α radiation and intensity measurements with a four-circle diffractometer (RIGAKU AFC-5 FOS) indicated systematic absence of reflections with $l = 2n + 1$ for $00l$ and $h = 2n + 1$ for $h00$, which are consistent with space group $P4_22_12$ of tetragonal symmetry. The cell parameters were determined by the least-squares method using 36 reflections (2θ = 20–28°, MoK_α, λ = 0.71069 Å) measured with a four-circle diffractometer.

MoK_α radiation monochromatized by pyrolytic graphite was used for intensity measurements. The intensities of reflections including crystallographically equivalent reflections within the range of $0 < 2\theta < 90°$ ($+h$, $+k$, $+l$) were obtained at room temperature by the $2\theta - \theta$ scan technique on a four-circle diffractometer. All the observed reflections were summarized in 317 unique reflections. Ninety-nine reflections having high standard deviations ($3\sigma_{hkl}(F_o) > |F_o|$) or unobservable intensities were eliminated from the least-squares refinement procedure, where $\sigma_{hkl}(F_o)$ is a standard deviation of each reflection obtained from counting statistics. Conventional Lorentz and polarization corrections were carried out in the

process of data collection. No absorption correction was made because of the small value of μr (<0.02).[1]

All computations in the present study were carried out using the programs referred to previously (*4*). Atomic scattering factors for Li, B, and N were taken from "International Tables for X-Ray Crystallography" (*5*).

Complex impedances of the sintered polycrystalline samples were measured in the range 5 Hz to 500 kHz using a vector impedance meter (HP 4800A). Carbon or Ag paste was used as electrodes. Specimens were placed under vacuum or Ar atmosphere.

Results and Discussion

Phases in the Li_3N–BN System

Table I shows the phases observed in the present preparations in the Li_3N–BN binary system. Most of the products showed the presence of α-Li_3BN_2. α-Li_3BN_2 could be obtained unaccompanied by other kinds of nitrides from the mixture of Li_3N/BN = 1.0–1.1 in molar ratio at 1070 and 1270 K. The product heated up to 1270 K showed a glassy white surface and did not hold the shape of the initial pellet of the starting mixture. Other products were white polycrystalline pellets. β-Li_3BN_2 could be prepared only in the case of heating up to 1170 K. X-ray powder diffraction data for the product of No. 3 in Table I are shown in Table II(c) in comparison with the values in the previous studies (*1, 2*).

Table II(d) lists the values calculated from single-crystal data of α-Li_3BN_2 shown later in the present manuscript. The calculated intensities were obtained from $I_{calc} = F^2M/L$, where F is the single-crystal structure factor, m is the multiplicity of crystal planes of a set of hkl values, and L is the combined Lorentz and polarization factor. The observed data agreed well with the calculated results except for the reflection at 2.67 Å. Intensity of this reflection was much smaller than the value reported by DeVries and Fleisher (*2*). The d-value corresponds to that of the (111) plane of Li_2O listed in Table II(e). The Li_2O content was estimated as 0.5–1 wt% using the method of standard addition on X-ray diffractometry.

Another compound represented as Li–BN in Table I was synthesized from the mixtures in the compositional range of $Li_3N/BN < 1.0$. However, its single phase could not be obtained in the present study. Its X-ray powder diffraction data are given in Table II(f). These diffraction lines were relatively broad in comparison with those of the coexisting phases in the products. They could not be indexed at the moment. The reflections at 3.81 and 2.24 Å in Table II(a) and 3.73 and 2.22 Å in Table II(b) may correspond to those at 3.75, 2.23, and 2.21 Å of the Li–BN compound.

Boron nitride has a layered structure analogous to that of graphite. The interlayer distances are 3.33 and 3.348 Å respectively in BN (*6*) and in graphite (JCPDS 26-1079). The spacing of 3.75 Å in Li–BN is comparable to the interlayer distance of 3.70 Å in lithium intercalated graphite, C_6Li (*7*). The structural similarity between graphite and boron nitride led Croft to attempt the preparation of boron nitride intercalation compounds (*8*). Catalytic activity was examined on additional compounds of boron nitride with K, Rb, and Cs (*9*). However, there still remains some ambiguity

[1] See NAPS document No. 04443 for 6 pages of supplementary material. Order from ASIS/NAPS, Microfiche Publications, P.O. Box 3513, Grand Central Station, New York, NY 10163. Remit in advance $4.00 for microfiche copy or for photocopy, $7.75 up to 20 pages plus $.30 for each additional page. All orders must be prepaid. Institutions and organizations may order by purchase order. However, there is a billing and handling charge for this service of $15. Foreign orders add $4.50 for postage and handling, for the first 20 pages, and $1.00 for additional 10 pages of material, $1.50 for postage of any microfiche orders.

TABLE II

X-RAY POWDER DIFFRACTION DATA

(a)		(b)		(c)		(d)			(e)			(f)	
d (Å)	I	d (Å)	I/I_o	d (Å)	I/I_o	hkl	d (Å)	I/I_o	hkl	d (Å)	I/I_o	d (Å)	I
3.81	m	3.73	10									3.75	vs
3.50	s	3.47	50	3.48	47	101	3.481	45					
		3.27	10	3.29	4	110	3.283	5					
2.82	vs	2.78	100	2.78	100	111	2.785	100					
		2.67	20	2.67	5				111	2.664	100	2.65	vw
2.63	s	2.63	30	2.63	24	002	2.630	28	200	2.306	8	2.23	w
2.24	w	2.22	5									2.21	w
2.07	vs	2.07	15	2.08	8	210	2.077	11				2.07	vw
		2.05	25	2.05	32	112	2.053	34				2.06	w
1.93	w	1.91	5	1.93	1	211	1.932	1				1.91	w
1.83	w												
1.74	vw	1.74	10	1.74	8	202	1.740	11					
		1.69	5										
1.64	vs	1.64	20	1.64	16	220	1.641	19				1.64	vw
						103	1.640	1					
		1.63	10	1.63	9	212	1.630	4	222	1.631	40		
				1.567	1	221	1.567	1					
1.55	m	1.55	10	1.546	5	113	1.546	9					
1.48	w			1.486	2	301	1.485	4					
						310	1.468	0.2					
1.42	w			1.415	3	311	1.414	5					
1.40	w			1.392	3	222	1.393	4	311	1.391	16		
1.32	w			1.316	2	004	1.315	5					
						320	1.288	0.5					
1.29	w			1.283	2	312	1.284	6					
1.25	w			1.252	2	321	1.251	7					

Note. (a) Li_3BN_2 from Goubeau and Anselment (*1*). (b) Li_3BN_2 from DeVries and Fleischer (*2*). (c) $Li_3BN_2(\alpha)$ + (Li_2O, 1 wt%) prepared at 1070 K in the present study. (d) $Li_3BN_2(\alpha)$ calculated from the result of a single-crystal. study (e) Li_2O from JCPDS card. (f) Li–BN prepared at 1340 K in the present study.

about the presence of boron nitride intercalation compounds because of the difficulty of preparation and identification.

Phase Relation between α- and β-Li_3BN_2

Single crystals of β-Li_3BN_2 were picked up from the inside of the product obtained by slow cooling of a melt at a rate of 1.5–3.0 K/hr from 1200 to 1000 K. Its DTA traces are illustrated in Fig. 1a. No thermal event appeared below 1100 K in the case of raising temperature at a rate of 20 K/min. An endotherm started at 1189 K was probably due to a melt. A very sharp exothermic peak was observed between 1136 and 1144 K on cooling the melt at a rate of 20 K/min. The exotherm began at 1160 K at the cooling speed of 2 K/min. The samples had changed to polycrystalline α-Li_3BN_2 after the DTA experiments.

Figure 1b shows the DTA curves of α-Li_3BN_2 containing less than 1 wt% Li_2O as an impurity. During the heating at a rate of 20 K/min, endothermic change started at 1111 K and its maximum was at 1195 K. On cooling the melt at a rate of 2 K/min, a

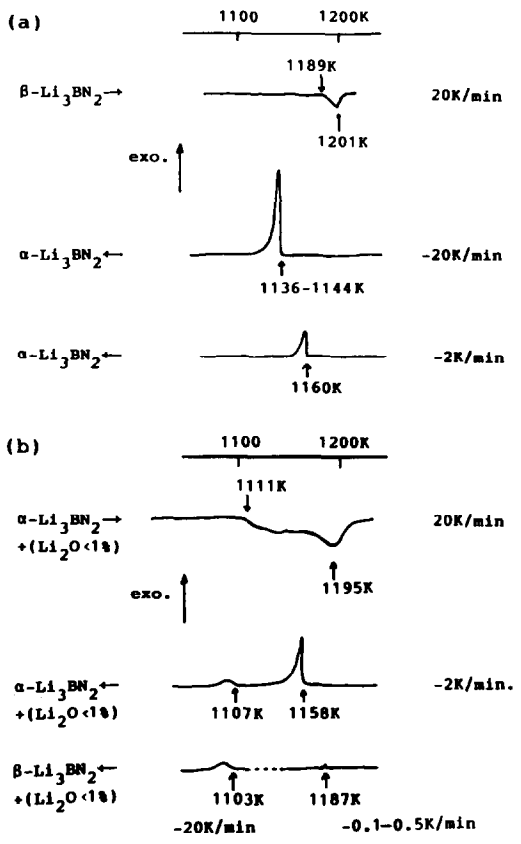

FIG. 1. Differential thermal analyses of (a) β-Li_3BN_2 single crystals (0.3–1.0 mm) and (b) polycrystalline α-Li_3BN_2 containing <1 wt% Li_2O.

sharp exotherm at 1158 K was followed by a small exothermic peak at 1107 K. The product remained a mixture of α-Li_3BN_2 and a small amount of Li_2O. β-Li_3BN_2 was obtained by an extremely slow cooling at a rate of 0.1–0.5 K/min to 1150 K and a successive cooling at a rate of 20 K/min to room temperature. A very small exothermic peak was detected at 1187 K. It corresponds to the melting point of a β-Li_3BN_2 single crystal shown in Fig. 1a. Another small exotherm also appeared at 1103 K. These DTA results lead to the conclusion that α-Li_3BN_2 crystallizes below 1160 K and β-Li_3BN_2 has a melting point around 1189 K. The small exothermic peak which appeared around 1107 K is considered as the eutectic temperature of the Li_3BN–Li_2O binary system.

Both α- and β-Li_3BN_2 were annealed at the desired conditions shown in Table III and quenched to room temperature in order to study the phase relations between them. Compressed pellets of β-Li_3BN_2 powder transformed completely to α-Li_3BN_2 maintaining the initial pellet form at 973 and 1088 K. However, no transition occurred in the case of β-Li_3BN_2 single crystals. The velocity of transformation probably depends on the crystal size. The phase transition of α- to β-Li_3BN_2 was caused by heating above 1140 K. The initial form of the α-Li_3BN_2 pellet was also held in all the runs shown in Table III. The reversible transition temperature between α- and β-phases can be estimated as around 1135 K. This phase transition could not be detected clearly by DTA. The transformation may partly contribute to the broad endothermic signal between 1111 and 1195 K shown in Fig. 1b, although the endothermic peak of transition could not be resolved from that of melting.

Figure 2 illustrates schematic free energy curves for the Li_3BN_2 phases against temperature. The high-temperature phase, β-Li_3BN_2, is obtained by slow cooling of the liquid. Free energy of the cooled melt

TABLE III

HEAT TREATMENTS OF α- AND β-Li_3BN_2

	T (K)	Time	Product
β-Li_3BN_2[a]	1173	10 min	β-Li_3BN_2
	1023–1093	50 hr	β-Li_3BN_2
β-Li_3BN_2[b]	1088	1 hr	α-Li_3BN_2
	973	1 hr	α-Li_3BN_2
	1160	10 min	β-Li_3BN_2
	1150	10 min	β-Li_3BN_2
α-Li_3BN_2	1140	10 min	β-Li_3BN_2, α-Li_3BN_2
	1130	10 min	α-Li_3BN_2
	1073	70 min	α-Li_3BN_2

[a] Single crystal (0.3–1.0 mm).

[b] Powder.

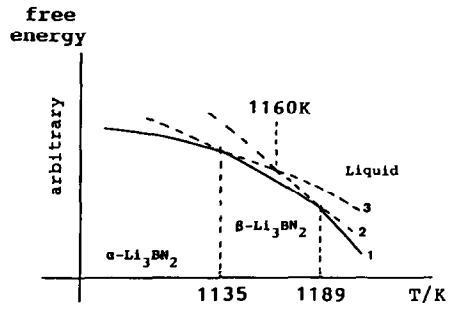

FIG. 2. Schematic free energy curves of Li_3BN_2 against temperature. The lines numbered 1 to 3 respectively represent free energy changes of liquid, β-Li_3BN_2 and α-Li_3BN_2.

changes along the solid lines. On rapid cooling the liquid is supercooled even in the β-phase stable region. Free energy changes along the dashed lines. As observed in the DTA of Fig. 1a, the α-phase, which is the low-temperature phase, is directly crystallized from the liquid even at 1160 K, which is in the β-phase stable region.

Crystal Structure of α-Li_3BN_2 and Its Comparison to the Related Structure

Crystallographic data are compared between α- and β-Li_3BN_2 in Table IV. The low-temperature phase, α-Li_3BN_2, has a higher symmetry and a little higher density

TABLE IV

CRYSTALLOGRAPHIC DATA

	α-Li_3BN_2	β-Li_3BN_2 (4)
	Tetragonal	Monoclinic
Space group	$P4_22_12$	$P2_1/c$
a =	4.6435(2) Å	5.1502(2) Å
b =	4.6435(2) Å	7.0824(2) Å
c =	5.2592(5) Å	6.7908(2) Å
β =		112.956(2)°
V =	113.40 Å^3	228.08 Å^3
D_{obs} =	1.75 Mg m^{-3}	1.74 Mg m^{-3}
D_{calc} =	1.747 Mg m^{-3}	1.737 Mg m^{-3}
μ =	0.082 mm^{-1}	0.082 mm^{-1}
Z =	2	4

TABLE V

FINAL ATOMIC COORDINATES WITH esd's

Atom	Position	X	Y	Z
Li(1)	$2b$	0	0	$\frac{1}{2}$
Li(2)	$4d$	0	$\frac{1}{2}$	$\frac{1}{4}$
B	$2a$	0	0	0
N	$4f$	0.2962(3)	0.2962(3)	$\frac{1}{2}$

than those of the β-phase. A model of the structure for α-Li_3BN_2 was obtained directly by placing all atoms in special positions of the $P4_22_12$ space group. The initial value for the x parameter in the $4f$ site was estimated by considering the bond lengths of B–N observed in β-Li_3BN_2 (*4*). The final full-matrix least-squares refinement gave agreement factors of $R = 0.042$ ($R = \Sigma||F_o| - |F_c||/\Sigma|F_o|$) and $Rw = 0.037$ {$Rw = [\Sigma w(|F_c| - F_o|)^2/\Sigma w|F_o|]^{1/2}$, where $w = 1/\sigma^2_{hkl}(F_o)$}. The final positional parameters are given in Table V.

The unit cell of α-Li_3BN_2 is shown in Fig. 3 by thermal vibration ellipsoids. The structure contains $(NBN)^{3-}$ ions as expected by Goubeau and Anselment (*1*). Boron atoms construct an elongated body-centered lat-

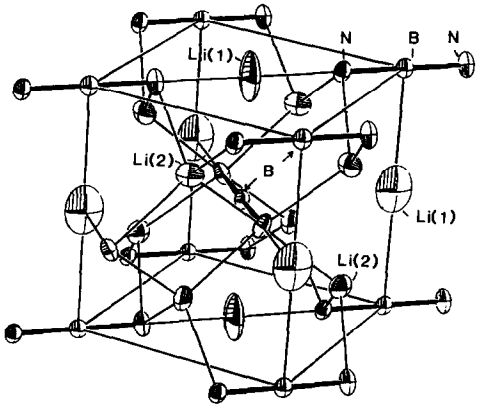

FIG. 3. Unit cell of α-Li_3BN_2. Thermal vibration ellipsoids of 70% probability for all atoms are shown. The straight N=B=N bonds are represented by thicker lines which denote covalent B=N bonds.

TABLE VI
INTERATOMIC DISTANCES (Å) AND ANGLES (°) WITH esd's

$B^{(i)}$–N	1.339(2)
Li(1)–N	1.945(8)
Li(2)–N	2.125(19)
Li(2)–$N^{(ii)}$	2.125(18)
N–$B^{(i)}$–$N^{(iii)}$	180
N–Li(1)–$N^{(iv)}$	180
N–Li(2)–$N^{(v)}$	103.6(2)
N–Li(2)–$N^{(ii)}$	112.5(9)

(i) $\frac{1}{2} - X, \frac{1}{2} + Y, \frac{1}{2} - Z$
(ii) $-\frac{1}{2} + Y, \frac{1}{2} - X, -\frac{1}{2} + Z$
(iii) $1 - X, 1 - Y, Z$
(iv) $-X, 1 - Y, Z$
(v) $-X, 1 - Y, Z$

tice. Each boron atom is linearly coordinated with two nitrogen atoms. The B–N bond length is 1.339 Å as shown in Table VI. The value agrees well with 1.339 and 1.336 Å in β-Li_3BN_2. A maximum residual electron density of 0.4 e $Å^{-3}$ appeared along the B–N bond in the final differential synthesis as in the case of β-Li_3BN_2 (*4*). It suggests the covalency of the B–N bond. Figure 4a illustrates the packing of $(NBN)^{3-}$ ions on the X–Y plane at $Z = 0$ and $\frac{1}{2}$. The direction of $(NBN)^{3-}$ ions in the $Z = 0$ plane is orthogonal to that in $Z = \frac{1}{2}$.

Lithium ions occur in two crystallographically different sites. Lithium (1) is coordinated linearly with two nitrogen atoms of two neighboring $(NBN)^{3-}$ ions in the same X–Y plane as shown in Figs. 3 and 4a. Li(2) is situated between the $Li^+(1)(NBN)^{3-}$ layers and is tetrahedrally coordinated with four N atoms. The tetrahedron is slightly elongated in the direction of the Z-axis. Lithium nitride, Li_3N, has some similarities to α-Li_3BN_2 in the position of lithium ions. It has 2-coordinated lithium ions between $(Li_2N)^-$ layers. One-half of the interlayer distance of 1.94 Å in Li_3N (*10*), which corresponds to the Li–N distance, coincides with the observed value 1.945 Å for Li(1)–N in α-Li_3BN_2 represented in Table VI. The Li(2)–N distance of 2.125 Å is comparable with the Li–N distance of 2.13 Å within the $(Li_2N)^-$ layer of Li_3N.

α- and β-Li_3BN_2

The crystal structure of α-Li_3BN_2 is compared with that of β-Li_3BN_2 in Fig. 5. The plane containing N=B=N and Li(1) of the α-phase corresponds to the array of N(1)=B=N(2) and Li(3) parallel to the X–Y plane of the β-phase. The interlayered Li(2) of the α-phase is related to Li(1) and Li(2) of the β-phase. The flat layer of N=B=N in α-Li_3BN_2 is due to the presence of 2-coordinated lithium ions. The layer in the β-phase is relatively puckered. All lithium ions are tetrahedrally coordinated with nitrogens in β-Li_3BN_2. The tetrahedrons around Li(1) and Li(2) are fairly distorted as represented previously (*4*).

The $(NBN)^{3-}$ units are closely packed in

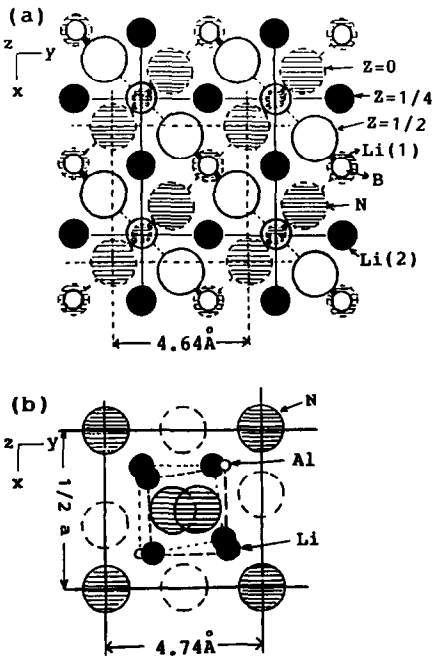

FIG. 4. Comparison of the structure: (a) projection of the α-Li_3BN_2 structure along the Z-axis and (b) projection of the antifluorite structure unit of Li_3AlN_2.

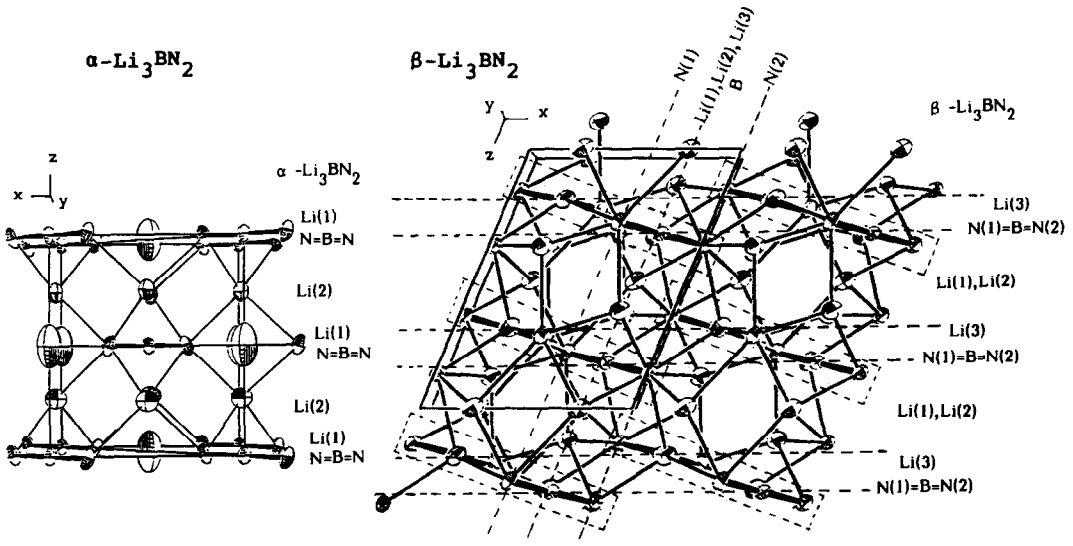

FIG. 5. Perspective views along [010] of the structure of α- and β-Li_3BN_2.

the low-temperature phase, α-Li_3BN_2, as illustrated in Fig. 4a. The packing seems to require the 2-coordinated lithium ion to link the units. The $(NBN)^{3-}$ ions reorient at the phase transition from α to β. The rotation causes a change of coordination number around this lithium ion. The 2-coordinated Li(1) in the α-phase corresponds to the tetrahedrally surrounded Li(3) in β-Li_3BN_2. As far as the interlayered lithium ions are concerned, their coordinations are always tetrahedral in both α- and β-phases. However, the tetrahedrons in the β-phase are squashed. The $(NBN)^{3-}$ packing is looser in the high-temperature phase, β-Li_3BN_2, than in the α-phase, probably because the $(NBN)^{3-}$ ions reorient for all lithium ions to take tetrahedral coordination. The low-temperature phase, α-Li_3BN_2, has a density a little higher than that of the high-temperature phase, β-Li_3BN_2.

α-Li_3BN_2 and Li_3AlN_2

The structure of Li_3AlN_2 is a superstructure of distorted antifluorite. Figure 4b schematically illustrates one-eighth of the cubic unit cell, which is closely related to an elemental cell of the antifluorite type. Anions basically pack in a face-centered cubic lattice. Cations are in tetrahedral sites. The tetrahedra are distorted because of the size difference between Li^+ and Al^{3+}. Nitrogen ions are at the levels of $Z = 0, \frac{1}{4}, \frac{1}{2}, \frac{3}{4}$, and 1 of the one-eighth cell. Nitrogen ions on the corners of the elemental cell superimpose on each other along the Z-axis in Fig. 4b. However, the positions of nitrogen, which should be located at the face center, shift to off-center.

The square enclosed by the dashed line in Fig. 4a represents the face-centered arrangement of nitrogen ions in α-Li_3BN_2. From the viewpoint of nitrogen packing, the α-phase can be related to Li_3AlN_2 of an antifluorite structure. The Li(2) is tetrahedrally surrounded by nitrogens as in the case of Li_3AlN_2. Different arrangements are seen around B and Li(1) compared with those around Al and Li in Li_3AlN_2. Both B and Li(1) ions are linearly coordinated by two N ions and situated on the edges of nitrogen tetrahedra. On the other hand, Al

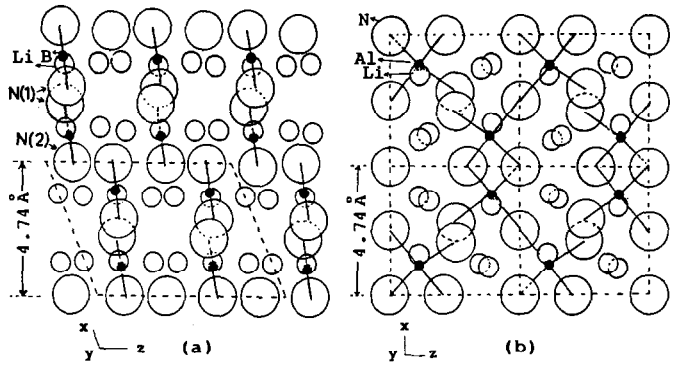

FIG. 6. Comparison of the structures: (a) projection of the β-Li_3BN_2 structure along the *Y*-axis and (b) projections of the Li_3AlN_2 structure along the *Y*-axis.

and Li ions in Li_3AlN_2 are at the centers of nitrogen tetrahedra. Consequently, half of the tetrahedral site is vacant in α-Li_3BN_2.

β-Li_3BN_2 and Li_3AlN_2

Projections shown in Fig. 6 reveal the contrast of structures between β-Li_3BN_2 and Li_3AlN_2. The distance between the N(2) layers in β-Li_3BN_2 is 4.74 Å, which agrees with one-half of the lattice constant of Li_3AlN_2 (a = 9.470 Å) (*3*). Arrays of Li, B, and N(2) ions in β-Li_3BN_2 correspond to those of Li, Al, and N ions in Li_3AlN_2. However, the nitrogen ions in β-Li_3BN_2 cannot keep the face-centered cubic packing in Li_3AlN_2 because of the presence of linear N–B–N units. The tetrahedra around lithium are also fairly distorted in β-Li_3BN_2. The structure of β-Li_3BN_2 is more open than that of Li_3AlN_2.

Li_2CN_2 and Li_3BN_2

We have considered the structures of α- and β-Li_3BN_2 compared with the antifluorite structure of Li_3AlN_2. They can also be related to the structure of Li_2CN_2, which is composed of Li^+ and $(NCN)^{2-}$ ions (*11*). The carbon atom is linearly coordinated by two nitrogen atoms. The $(NCN)^{2-}$ ion is centrosymmetric and the bond length is 1.23 Å. The $(NCN)^{2-}$ ions are located at the corners and at the body center of a tetragonal lattice. Each Li^+ ion is at the center of a squashed tetrahedron of N atoms.

Ternary lithium nitrides containing the elements in the third line of the periodic table (Mg^{12}, Al^3, Si^{13} and P^{14}) crystallize in the antifluorite-type crystal structure. The third elements are tetrahedrally coordinated with nitrogen. In cases of the second line elements such as B and C, the structure is characterized by the presence of linear $(NBN)^{3-}$ and $(NCN)^{2-}$ anion groups. High covalencies are expected for the bondings in the groups from the residual electron densities of difference-Fourier synthesis and also from the short bond lengths.

Ionic Conductivities of α- and β-Li_3BN_2

Figure 7 illustrates examples of complex impedance diagrams for polycrystalline sintered samples of α- and β-Li_3BN_2. Conductivities were estimated from the values of intersections of extrapolated semicircle and real axis. They are plotted in Fig. 8. The conductivity of the high-temperature phase, β-Li_3BN_2, was a little higher than that of the low-temperature one, α-Li_3BN_2, at 400 K. Electronic conductivities were measured by the dc method using carbon as the electrodes. The electronic contributions

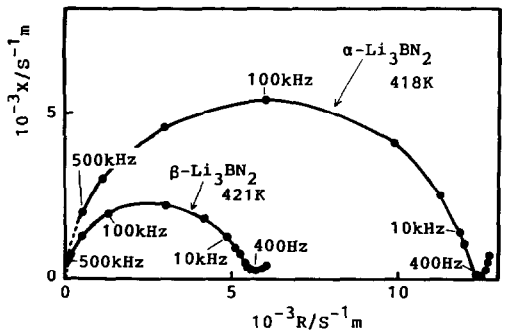

FIG. 7. Complex impedance plots for polycrystalline α-Li_3BN_2 at 418 K and for β-Li_3BN_2 at 421 K.

were less than 1% of the total conductivities around 500 K for both samples.

The activation energy of β-Li_3BN_2 (64 kJ/mole) was smaller than that of α-Li_3BN_2 (78 kJ/mole). The difference in activation energy should be discussed in relation to the crystal structure, especially the coordination number, the configuration around lithium ions, the size of the bottleneck for ionic conduction, etc. α-Li_3BN_2 has one-third of the Li in 2-coordination site and two-thirds of the Li in a tetrahedral site. β-Li_3BN_2 has all lithiums in a tetrahedral site. We have no information about the diffusion of migration paths of lithium ions in the crystal structure. Thus it is quite difficult to estimate the size of the bottleneck for the ionic conduction.

Anisotropies of ionic conduction should be expected from consideration of the crystal structures. It might contribute to the elongation of the semicircle along the real axis as shown in Fig. 7. However, we could not obtain single crystals with an adequate size for conductivity measurements.

In summary, phase relations between α- and β-Li_3BN_2 were studied. β-Li_3BN_2 was the high-temperature phase stable above 1135 K. The analyzed crystal structure of α-Li_3BN_2 was characterized as a close packing of linear $(NBN)^{3-}$ ions. It was a lithium ionic conductor having conductivity of 3×10^{-5} S m^{-1} at 400 K.

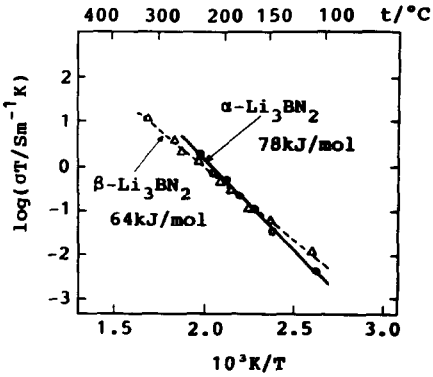

FIG. 8. Semilogarithmic plot of the conductivity σ times the absolute temperature T against the inverse absolute temperature.

Acknowledgments

The authors thank Professor F. Kanamaru and his colleagues at ISIR of Osaka University and also Professor H. Horiuchi at the University of Tokyo for their assistance in structural analysis. We also thank Mr. T. Tanaka for operating the intensity collection system on X-ray diffraction of MAC at ISIR. We thank the research group under the direction of Professor S. Kawai at ISIR for their technical assistance in the impedance measurements. This research was partly supported by a grant from the research project in ISIR on development of new materials for energy and also by a grant from the Casio Science Promotion Foundation.

References

1. V. J. GOUBEAU AND W. ANSELMENT, *Z. Anorg. Allg. Chem.* **310,** 248 (1961).
2. R. C. DEVRIES AND J. F. FLEISHER, *Mater. Res. Bull.* **4,** 433 (1969).
3. V. R. JUZA AND F. HUND, *Z. Anorg. Allg. Chem.* **257,** 13 (1948).
4. H. YAMANE, S. KIKKAWA, H. HORIUCHI, AND M. KOIZUMI, *J. Solid State Chem.* **65,** 6 (1986).
5. "International Tables for X-Ray Crystallography," Vol. IV, Kynoch Press, Birmingham, England (1974).
6. R. S. PEASE, *Acta Crystallogr.* **5,** 356 (1952).
7. D. BILLAND, E. MCRAE, AND A. HEROLD, *Mater. Res. Bull.* **14,** 857 (1979).
8. R. C. CROFT, *Austral. J. Chem.* **9,** 206 (1956).

9. C. MUGIYA, N. OHIGASHI, Y. MORI, AND H. INOKUCHI, *Bull. Chem. Soc. Japan.* **43,** 287 (1970).
10. A. RABENAU, AND H. SCHULZ, *J. Less-Common Met.* **40,** 155 (1976).
11. M. G. DOWN, M. J. HALEY, P. HUBBERSTEY, R. J. PULHAM, AND A. E. THUNDER, *J. Chem. Soc. Dalton Trans.* 1407 (1978).
12. V. R. JUZA AND F. HUND, *Z. Anorg. Allg. Chem.* **257,** (1948).
13. V. R. JUZA, H. H. WEBER, AND E. MEYER-SIMON, *Z. Anorg. Allg. Chem.* **273,** 48 (1953).
14. J. -F. BRICE, J. -P. MOTTE, A. E. MASLOUT, AND J. AUBRY, *C. R. Acad. Sci. Paris Ser. C* **273,** 744 (1971).